ATOMISTIC STUDIES OF PROPERTIES OF HELIUM IN BCC IRON USING THE NEW HE–FE POTENTIAL—David M. Stewart, Stanislav Golubov (Oak Ridge National Laboratory and the University of Tennessee), Yuri Ostesky, Roger E. Stoller, Tatiana Seletskaia, and Paul Kamenski (Oak Ridge National Laboratory)

SUMMARY

In fusion applications, helium caused by transmutation plays an important role in the response of RAFM steels to neutron radiation damage. We have performed atomistic simulations using a new 3-body Fe–He inter-atomic potential combined with the Ackland iron potential. With the ORNL potential, interstitial helium is very mobile and coalesces together to form interstitial clusters. We have investigated the mobility of these clusters. If the He cluster is sufficiently large the cluster can push out an Fe interstitial, creating a Frenkel pair. The resulting helium-vacancy cluster is not mobile. The ejected SIA is mobile, but is weakly trapped by the He–V cluster. If more helium atoms join the He–V cluster, more Fe interstitials can be pushed out, and they combine to form an interstitial dislocation loop. The reverse process is also studied. Multiple helium atoms can be trapped in a single vacancy, and if there are few enough, the vacancy can recombine with an Fe interstitial to create a helium interstitial cluster. These mechanisms are investigated together in larger simulations that examine the nucleation of He defects. Results are compared based on temperature, interatomic potentials used and helium concentration. Helium bubbles of sizes 1-6nm are also studied.

PROGRESS AND STATUS

Introduction

Helium produced in neutron irradiated iron plays an important part in its mechanical properties. The growth, migration and coalescence behavior of helium bubbles is very sensitive to the properties of individual He interstitials and helium-vacancy clusters [1]. A new He–Fe inter-atomic potential has been developed at ORNL, based on extensive fitting to first-principles calculations of point defects and clusters [2–5]. This potential has been used to investigate the properties of helium and helium-vacancy clusters in MD and MS simulations.

Helium diffuses very fast in the matrix, but is easily trapped in vacancies [6]. It is possible for a self-interstitial to recombine with the vacancy, kicking the helium back into an interstitial position. Previous calculations [5] showed that recombination is possible not only for a single substitutional He, but even when the vacancy contains multiple Helium atoms. If the vacancy contains 5 or less atoms, it is found to be energetically favorable for it to recombine with the SIA to form a helium interstitial cluster. For 6–8 atoms there is no clear winner, and for more than 8 it is more favorable for the SIA to be trapped close to a He–V cluster without recombining with it.

A dynamic simulation of a He_8 interstitial cluster at 600K showed that the reverse process (i.e. Frenkel pair formation) can happen—an iron atom is pushed out of its lattice site, creating a He_8V cluster and an SIA. The SIA was trapped beside the cluster.

Simulation Method

The general procedure followed is: Generate perfect BCC lattice. Introduce the defect(s) to be studied. Relax at constant volume using a mixture of conjugate gradient and simulated annealing, and save the atom positions in units of the lattice constant. Start the MD simulation.

The MD simulations used NVE dynamics. The lattice constant and initial velocities were chosen to give close to zero pressure and the desired initial temperature. The boundary conditions are periodic in X, Y and Z, which are $\langle 100 \rangle$ directions. The velocity Verlet algorithm with a timestep of 0.3fs is used. As volume and temperature correction are not used, when processes that release energy are simulated the temperature and pressure both rise during the simulation.

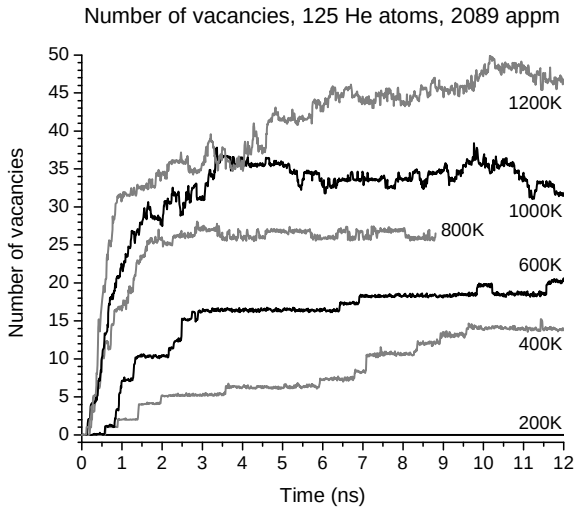

Figure 1. Vacancy production

Coalescence

The dynamic simulations described in the previous semiannual [5] that were run with 125 helium atoms in a 31×31×31 BCC iron matrix (60,000 iron atoms) were continued and the same trends continued. At 200K, the helium slowly and inexorably coalesced until it formed interstitial clusters too big to be mobile, up to a maximum of He_8 with no vacancies or SIAs. At 400K, an SIA is ejected when a cluster reaches 8 or 9 helium atoms, and no SIAs escaped their HeV cluster. At higher temperatures, smaller clusters like He_2 and He_3 were short lived; those that did form grew bigger since the number of available He atoms was fixed. The higher the temperature, the less He atoms were needed to eject an SIA, and the easier the SIAs escape, to be captured by larger clusters with SIAs. The number of vacancies is plotted as a function of time in Fig. 1. This is Fig. 1 in [5] extended with new data.

The simulations run with different potential combinations were also continued, shown in Fig. 2. (Fig. 3 from [5] extended). With Ackland + Wilson, Frenkel pairs formed much faster than with the ORNL potential, because an SIA can be ejected from an interstitial cluster of only 2 or 3 Heliums. The Mendelev + ORNL and Finnis-Sinclair + ORNL, and Mendelev + Juslin–Nordlund [10] combinations were all similar and formed bubbles at a rate and quantity that was between the other two combinations. For Ackland + Juslin–Nordlund [10] showed no clustering so is not plotted. The 976 appm simulations using a box of 40×40×40 were also continued, and the 600K run is shown in Fig. 3 (Fig. 4 from [5] extended). The bubbles took longer to form with the lower concentration, but the number and size distribution was similar.

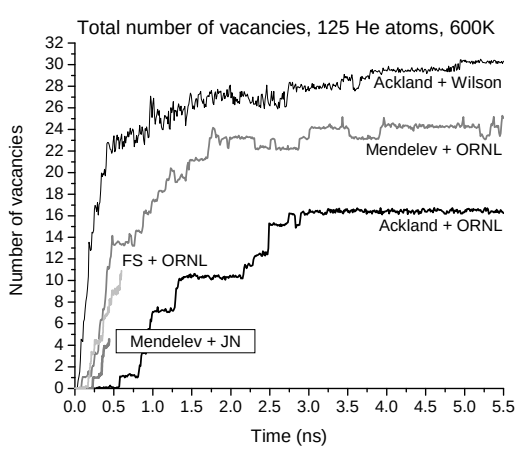

Figure 2. Coalescence for different potentials.

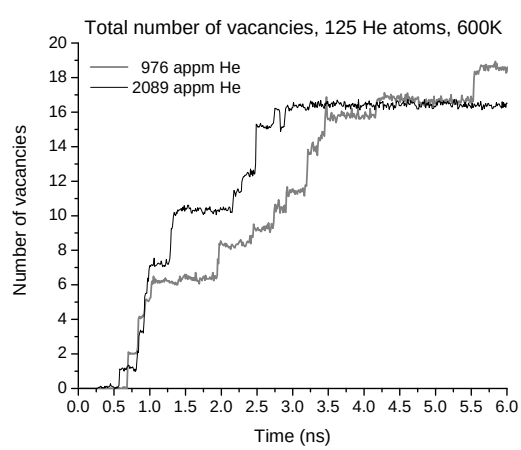

Figure 3. Coalescence for different box sizes.

Cluster Diffusion

The rate of diffusion of helium interstitial clusters was investigated in the previous semiannual [5] for three iron matrix potentials with the ORNL potential and the Wilson potential.

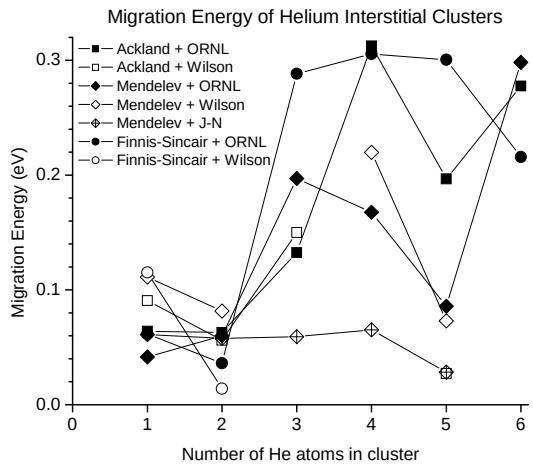

Figure 4. Migration energy results.

Here we add the Mendelev potential in combination with the Juslin-Nordlund potential. The energy barriers calculated from Arrhenius fits are added to the plot of energy barriers (Fig.6 in [5]), in Fig. 4. The Mendelev matrix with the Juslin–Nordlund potential showed consistently low barriers compared to the other combinations. The Juslin–Nordlund He–Fe potential with either of the other two matrix potentials predicts that all clusters will dissociate into individual interstitial Helium atoms, so there are no cluster diffusion rates for them.

Helium bubbles

The He–V defects nucleated in the coalescence simulation are nascent bubbles. We have also simulated larger ones. Bubbles of diameters of 1, 2, 4 and 6 nm were investigated. They consist of Helium atoms in a spherical void containing 59, 339, 2741 or 9577 vacancies respectively. Figure 5 shows a cross-section of a 4nm (2741 vacancy) bubble with a helium to vacancy ratio of one half.

The simulations used the Ackland Iron, the ORNL He–Fe, and the Aziz helium potentials. It was discovered that the helium stays a distance inside the bubble, leading to empty space between the He and the surface iron atoms. The gap was large enough that in these simulations our Fe–He potential is effectively a pair potential. The He atoms rarely come close enough to an iron atom to invoke the 3-body component of our potential, which has a range of 2.2Å.

Figure 6 shows the radial density function of a 2nm bubble with a He/V ratio of 0.49. The squares show the Iron atoms that make up the surface of the bubble. The circles represent the density of helium atoms in the space. The helium density oscillates enough to suggest a shell structure to the arrangement of atoms, but not enough to suggest solid helium. The dotted line in the figure, an approximation to a uniform distribution, shows that the actual helium density (1.04) is just over double the nominal density (0.49). The helium occupies a sphere of radius 7.7Å (just under half the volume of the void), and the gap is approximately 2.2Å.

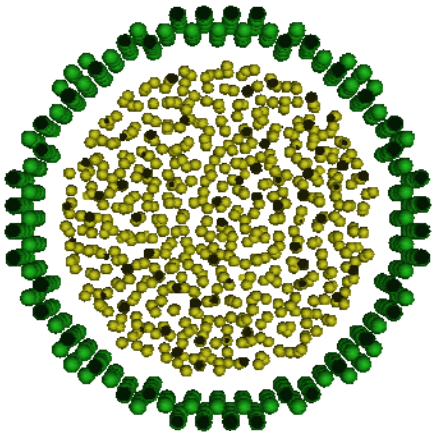

Figure 5. 4nm 0.5He/V bubble at 100K.

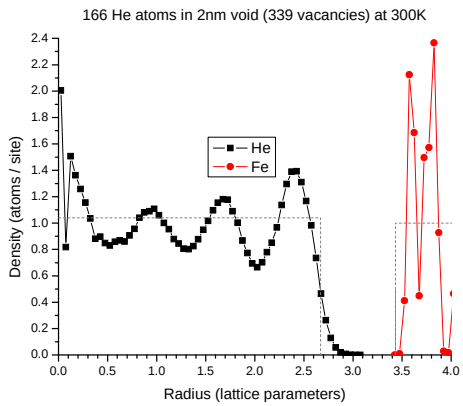

Figure 6. RDF of 2nm equilibrium bubble at 300K.

In a void, the surface matrix atoms move inwards slightly, reducing the volume of the void. At higher temperatures, they move in more. Adding helium to the void pushes the atoms outwards, increasing the volume slightly. The more helium added, the further the bubble expands. There is a point where this balances and the bubble is neither expanded nor contracted; the surface atoms are at the same place as they would be in a perfect lattice. We use this point as our condition for equilibrium. The equilibrium He/V ratio is temperature and size dependant. In general, the equilibrium He/V ratio is lower for higher temperatures and larger bubbles.

Figure 7 shows the dilation of a 2nm diameter bubble as a function of He/V ratio for different temperatures. The equilibrium ratio for each temperature can be determined by where it crosses the horizontal zero line. At 2nm, the curves for the different temperatures are close together; for larger bubbles, the curves spread out more (not shown).

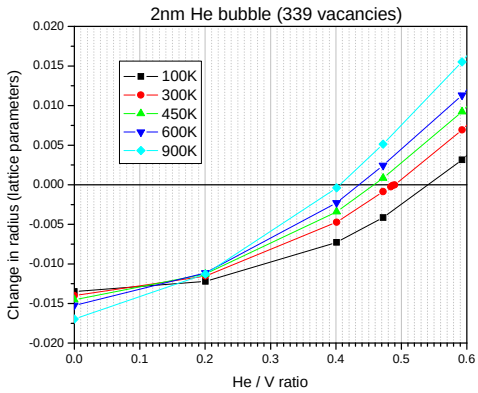

Figure 7. Dilation of 2nm bubbles with T.

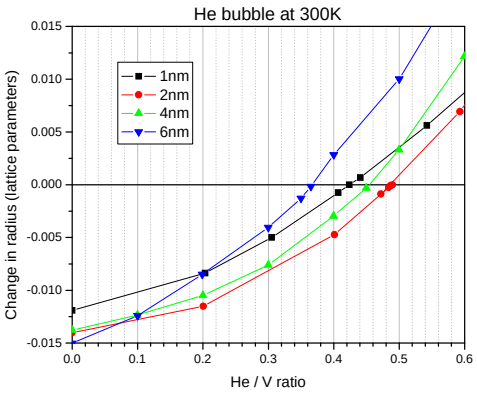

Figure 8. Dilation of different bubbles at 300K.

Increasing the temperature causes a void to shrink, but a bubble to grow. The higher the helium density the bigger this effect is. There is a crossover point where the bubble is relatively independent of temperature. This happens at lower densities than equilibrium, so the bubble is smaller than at equilibrium. The bigger the bubble the lower the He density this occurs at. In Figure 7, this can be seen where the lines almost come together at about 0.15He/V.

Figure 8 shows the dilation of different sized bubbles as a function of He/V ratio at 300K. They show equilibrium at smaller ratios as size increases, except for the 1nm bubble.

The bubble volume is defined by the position of the surface atoms. The volume actually occupied by helium is defined by the He atom positions, and is substantially smaller. Thus there are 2 ways to define helium density and helium pressure, depending on which volume is used. These are plotted in Figures 9 and 10 respectively. The squares show quantities calculated using the former definition; the circles the latter definition. As the smallest bubbles cram the helium into a tiny fraction of the space, the choice of which volume to use makes a huge difference. Note in Figure 11 that the helium density in non-monotonic if the entire bubble volume is used (as it was in the calculations in Figure 8).

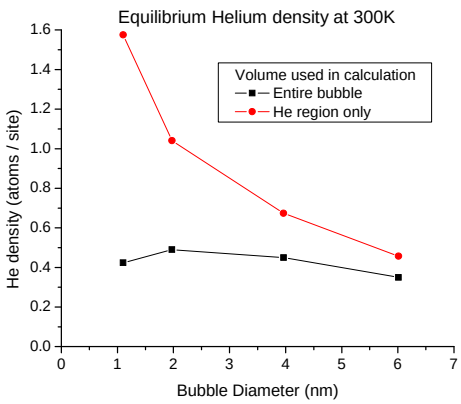

Figure 9. Eq. He Density of bubbles at 300K.

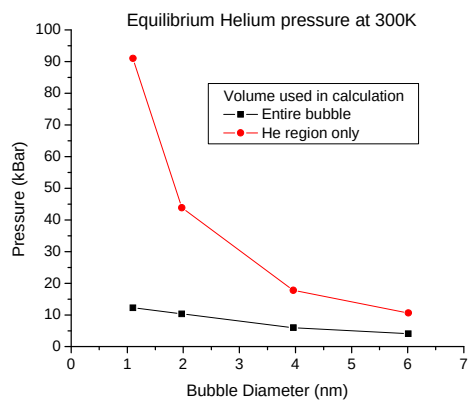

Figure 10. Eq. He Pressure of bubbles at 300K.

Effect of facets

Different crystallographic orientations have different surface energies, which is likely to affect the relationship between temperature, pressure and He/V ratio. In order to determine the effect of different crystallographic surfaces, simulations are being run with three different shaped Helium bubbles (in addition to the spherical ones).

Each void has a volume similar to the 339-vacancy 2nm spherical void. The volumes are different because each shape can only have an integer number of 'shells' of vacancies. The 1.5nm cubical void, which consists of only {100} surfaces, has 341 vacancies. The 2.5nm rhombic dodecahedral void (only {110} surfaces) has 369 vacancies. The 2.9nm octahedral void (only {111} surfaces) has 391 vacancies. Cross-sections of them are pictured in Figure 11.

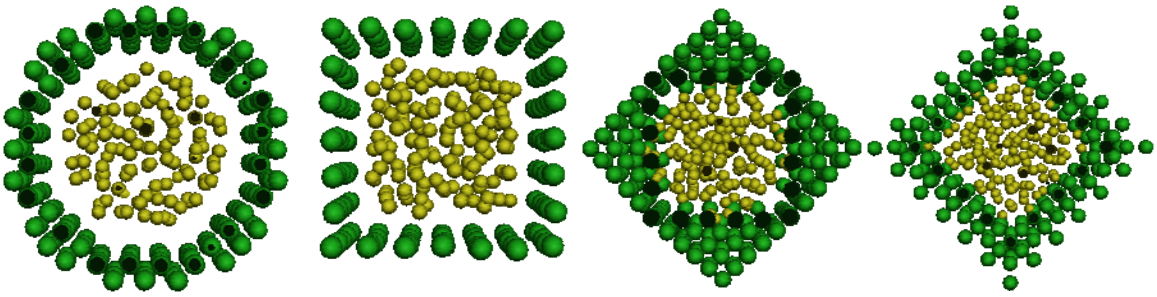

Sphere
All surfaces

Cube
{100} surfaces

Rhombic dodecahedron
{110} surfaces

Octahedron
{111} surfaces

Figure 11. The four different shapes of void being simulated. All 0.4He/V at 300K.

References

[1] S.I. Golubov, R.E. Stoller, S.J. Zinkle, and A.M. Ovcharenko, Kinetics of coarsening of helium bubbles during implantation and post-implantation annealing, Journal of Nuclear Materials 361 (2007), pp. 149–159.

[2] T. Seletskaia, Y.N. Osetsky, R.E. Stoller, and G.M. Stocks, Magnetic Interactions Influence the Properties of Helium Defects in Iron, Physical Review Letters 94 (2005), pp. 046403.

[3] T. Seletskaia, Y.N. Osetsky, R.E. Stoller, and G.M. Stocks, Calculation of helium defect clustering properties in iron using a multi-scale approach, Journal of Nuclear Materials 351 (2006), pp. 109–118.

[4] T. Seletskaia, Y.N. Osetsky, R.E. Stoller, and G.M. Stocks, Development of a Fe He interatomic potential based on electronic structure calculations, Journal of Nuclear Materials 367 (2007), pp. 355–360.

[5] D.M. Stewart, last semiannual report

[6] H. Trinkaus and B. Singh, Helium accumulation in metals during irradiation–where do we stand? Journal of Nuclear Materials 323 (2003), pp. 229–242.

[7] G.J. Ackland, D.J. Bacon, A.F. Calder, and T. Harry, Computer simulation of point defect properties in dilute Fe-Cu alloy using a many-body interatomic potential, Philosophical Magazine A-Physics of Condensed Matter Structure Defects and Mechanical Properties 75 (1997), pp. 713–732.

[8] M.I. Mendelev, S. Han, D.J. Srolovitz, G.J. Ackland, D.Y. Sun, and M. Asta, Development of new interatomic potentials appropriate for crystalline and liquid iron, Philosophical Magazine 83 (2003), pp. 3977–3994.

[9] W. Wilson and R. Johnson, Rare Gases in Metals, Interatomic Potentials and Simulation of Lattice Defects, Battelle Institute Materials Science Colloquia, 1972, 375-390 (1972).

[10] K. Nordlund and S. Dudarev, Interatomic potentials for simulating radiation damage effects in metals, Comptes rendus-Physique (2008).

[11] M.W. Finnis and J.E. Sinclair, A simple empirical N-body potential for transition metals, Phil. Mag. A 50 (1984), pp. 45–55.